Spectral analysis of atmospheric composition: application to surface ozone model-measurement comparisons.

Dene R. Bowdalo[1], Mathew J. Evans[1], and Eric D. Sofen[1]

[1]Wolfson Atmospheric Chemistry Laboratories, Department of Chemistry, University of York, Heslington, York, YO10 5DD, UK

Correspondence to: Dene Bowdalo (db876@york.ac.uk)

Abstract. Models of atmospheric composition play an essential role in our scientific understanding of atmospheric processes and in providing policy strategies to deal with societally relevant problems such as climate change, air quality and ecosystem degradation. The fidelity of these models needs to be assessed against observations to ensure that errors in model formulations are found and that model limitations are understood. A range of approaches are necessary for these comparisons. Here, we apply a spectral analysis methodology for this comparison. We use the Lomb-Scargle Periodogram, a method similar to a Fourier transform, but better suited to dealing with the gapped datasets typical of observational data. We apply this methodology to long-term hourly ozone observations and the equivalent model (GEOS-Chem) output. We show that the spectrally transformed observational data shows a distinct power spectrum with regimes indicative of meteorological processes (weather, macroweather) and specific peaks observed at the daily and annual timescales together with corresponding harmonic peaks at half, third etc. of these frequencies. Model output shows corresponding features. A comparison between the amplitude and phase of these peaks introduces a new comparison methodology between model and measurements. We focus on the amplitude and phase of diurnal and seasonal cycles and present observational/model comparisons and discuss model performance. We find large biases notably for the seasonal cycle in the mid-latitude northern hemisphere where the amplitudes are generally overestimated by up to 16 ppbv, and phases are too late on the order of 1-5 months. This spectral methodology can be applied to a range of model-measurement applications and is highly suitable for Multimodel Intercomparison Projects (MIPs).

1   Introduction

Ozone (O_3) at the surface is a pollutant, harmful to both human and plant health (WHO, 2005; Fowler et al., 2009). It is the dominant source of the hydroxyl radical (OH) (Levy, 1972), which controls the concentration of key climate gases (CH_4, HCFCs etc.) and is an important climate gas in its own right (Forster et al., 2007).

The main sources of O_3 in the troposphere are from photochemical production and transport from the stratosphere. It is lost through dry deposition and photochemical loss (Monks et al., 2000; Stevenson et al., 2006; Monks et al., 2015). In the troposphere O_3 photochemical production is driven by the emission of precursors: nitrogen oxides (NO_X), carbon monoxide (CO), methane (CH_4) and volatile organic compounds (VOCs) which in the presence of appropriately energetic photons can

lead to a complex set of reactions which ultimately produce O$_3$ in a non-linear fashion (Ehhalt, 1999; Jenkin and Clemitshaw, 2000; Monks, 2005).

Our understanding of tropospheric ozone comes from observations of the spatial and temporal distribution of ozone and its precursors together with numerical simulations. Given the lifetime of tropospheric ozone (~22 days) (Stevenson et al., 2006), global models either online (Chemistry Transport Models - CTMs) or offline (Earth System Models - ESMs) are particularly useful and are used extensively. An assessment of model fidelity is essential to find errors in processes, to evaluate where model processes are inadequate and to understand when models provide useful predictive capabilities.

Depending on the emphasis of the study, a range of methodologies have been applied to model-measurement comparisons for ozone. Many have used comparisons to 'long-term' surface ozone observations as a basis (Tanimoto et al., 2005; Jonson et al., 2006; Oltmans et al., 2006; Derwent et al., 2008; Cooper et al., 2012; Logan et al., 2012; Hess and Zbinden, 2013; Oltmans et al., 2013; Parrish et al., 2013, 2014). Typically, these observations are averaged onto a monthly timescale and compared to a similarly averaged model output, and the two compared as a function of time. This offers some advantages. The averaged measurement and modelled datasets are small, making comparisons compact and easy to understand. It also removes the short-term variability (< monthly) that may not be of interest to the researchers.

However, this approach also suffers from a range of limitations. Processes occurring on timescales shorter than the monthly include photochemistry, deposition, transport and emission, all of which are important to the success of the model. By focusing on the monthly variability alone other timescales are ignored which may lead to insufficiently robust analysis of model performance. What is required is a methodology to assess model fidelity on a range of timescales simultaneously. Spectral methods offer this approach but for atmospheric chemistry have only been used in a small number of studies, and specifically for ozone in a limited sense, fitting standalone sine waves to time series (Schnell et al., 2015) and applied to a small selection of coarse monthly average data (Parrish et al., 2016).

In this paper we introduce a methodology for the spectral analysis of observations of atmospheric composition data (Sect. 2). We describe this methodology for two contrasting sites (Sect. 3). We then show this methodology applied to a range of surface ozone observations sites (Sect. 4), and applied to a CTM (Sect. 5). We then compare these results and finally discuss potential reasons for biases (Sect. 6).

2   Spectral methods

The decomposition of a time-series into a set of orthogonal periodic functions was first suggested by Joseph Fourier. Classically this decomposition yields a number of sinusoidal waves each with an associated amplitude and phase. This technique is used extensively in disciplines such as engineering and geophysics. Using a computer to compute this decomposition, traditionally by correlation of basis functions with a time series, is termed the Discrete Fourier Transform (DFT). However, this method is computationally intense which led to the development of the Fast Fourier Transform (FFT). One of the limitations of the FFT is that it is cannot accurately handle datasets with irregular time intervals. Some kind of interpolation is needed to provide data on a regular time interval which biases results (particularly at high frequencies) (Press et al., 1992; Schulz and Stattegger, 1997;

Musial et al., 2011; Rehfeld et al., 2011). Atmospheric observations inherently have irregular time intervals due to instrumental issues (power breaks, instrument failures, calibration times etc.) so another numerical method is needed.

The Lomb-Scargle Periodogram (LSP) is a spectral analysis method designed to handle gapped datasets (Lomb, 1976; Scargle, 1982; Horne and Baliunas, 1986; Press and Rybicki, 1989; Press et al., 1992), which has been applied in a small
5   number of instances to air quality data (Dutton et al., 2010; Stefan et al., 2010). It can be formulated as a modified DFT (Scargle, 1982; Press et al., 1992), and also equivalently by the least squares of fit of sine and cosine waveforms to a time series centred around zero (Lomb, 1976). Using the modified DFT methodology, for an equally spaced time series, taking the magnitude squared of the dot products of a time series (centred around zero) with cosine and sine waveforms at set frequencies gives a spectrum that is an estimate of the power contributing to the original data. In the presence of data gaps, the sine and
10   cosine model functions are modified to be exactly orthogonal by an additional phase parameter Θ (Scargle, 1982), making the estimation invariant to shifts in time of the input time series (i.e. data gaps). It is commonly represented in its normalised form (termed Power Spectral Density), e.g (Press et al., 1992), as:

$$P(\omega) = \frac{1}{2\sigma^2} \left(\frac{\left[\sum_{i=1}^{N} y(t_i) \cos\left(\omega t_i - \Theta\right) \right]^2}{\sum_{i=1}^{N} \cos^2\left(\omega t_i - \Theta\right)} + \frac{\left[\sum_{i=1}^{N} y(t_i) \sin\left(\omega t_i - \Theta\right) \right]^2}{\sum_{i=1}^{N} \sin^2\left(\omega t_i - \Theta\right)} \right) \tag{1}$$

where $y(t_i)$ is the observable at time t_i, ω is the angular frequency, and σ^2 is the variance of the time series. The phase offset
15   Θ is calculated with the four quadrant inverse tangent, shown by Eq. (2). Additionally, the DFT is modified so when data gaps exist the distribution of the normalised spectrum for pure Gaussian noise is exponential, equivalent to that of the equal spaced case.

$$\Theta = \frac{1}{2} \arctan\left(\sum_{i=1}^{N} \sin\left(2\omega t_i\right), \sum_{i=1}^{N} \cos\left(2\omega t_i\right) \right) \tag{2}$$

The LSP does not output any phase information natively. However, Hocke (1998) gave a method to modify the LSP algorithm
20   to output real and imaginary components or amplitude and phase, as resultant from the Fourier transform, which we apply in our work.

2.1 Spectral leakage

There are some problems in accurately identifying the amplitude and phase of periodic components. The main issue is termed 'spectral leakage'. Typically, Lomb-Scargle methods calculate power at integer frequencies equally spaced between 1 (total
25   span of time series) and one-half of the average sampling frequency (termed 'average Nyquist frequency'), reflecting the Fourier frequencies. If strong periodicity exists on a frequency, not an integer integral on the span of the time series, then its power would lie between two of the frequencies, resulting in leakage of that power throughout the rest of the spectrum. Atmospheric time series are not typically integer year long. For example, if the time series was 10.5 years long the spectrum

would consist of the periods: 10.5, 5.25, 3.5, 2.1, ...,1.16 1.05, 0.955 years etc. Therefore, if large variability were contained on exactly a 1 year cycle, the LSP would spread that power throughout the spectrum.

Spectral leakage results from an assumption in spectral analysis methods that the time record is infinitely long. The transform assumes that the finite dataset is one period of an infinite periodic signal. Therefore, when the periodicity of interest is non-harmonic with the total span of the time record, there is a discontinuity, which results in leakage in the spectral domain (Horne and Baliunas, 1986).

To ensure the power leakage from multiple periodic components does not contaminate the entire spectrum, the input time series can be multiplied by a window function (Harris, 1978). The window is shaped so that it is zero at beginning and end, and has some defined shape in between. The window effectively changes the shape of the leakage in the frequency domain, limiting its impact to only a few frequencies around the peak frequency, providing a trade-off between peak resolution (the width of the peak) and spectral leakage (the amplitude of the tails of the leakage), with different windows altering the peaks of the spectrum in different ways. In this study a Hanning window was chosen as it offers an acceptable trade-off between resolution and spectral leakage (Harris, 1978).

Although the shape of the leakage can be altered, the peak amplitude will still be underestimated as there are no frequencies that estimate exactly at the exact frequency of interest. However, the LSP methodology (unlike the FFT) can estimate at any frequency, allowing the exact capturing of the top of the peak. Thus, if significant cycles are known a-priori (e.g. annual, daily etc.) their sinusoids can be calculated very accurately.

3   Lomb-Scargle Periodogram of surface ozone

Figure 1 shows the time series of hourly surface ozone mixing ratios collected at Cape Verde (Carpenter et al., 2010) and Lompoc together with equivalent model output (see Sect. 5). Cape Verde (16.51° N, 24.52° W), is a small remote island country consisting of 10 islands situated in the tropical eastern North Atlantic Ocean, 570 km off the West African coast. It represents one of the only ozone measurement stations in the tropics, and is relatively undeveloped, making it one of the small number of baseline oceanic measurement sites also. It is maintained by the atmospheric chemistry group at the University of York, and thus presents a readily available dataset for analysis. Lompoc (34.73° N, 120.43° W), is a EPA AQS rural continental site located on the US Californian west coast. Using the Lomb-Scargle methodology, the time series at Cape Verde and Lompoc can be transformed into a number of sinusoidal waves at a range of periods with differing amplitudes and phases. In Fig. 2 we show the amplitude (ppbv) of these waves as a function of their period (days).

The spectra for both sites shown in Fig. 2 have a range of characteristic features. There are broadly linear regions from 2 hours to 10 days and from 10 days to the last period of 1826 days. There are also sets of peaks which occur at characteristic timescales (i.e. 1 day and 1 year). We will initially discuss the identification of these linear regimes and then discuss the identification of the peaks.

3.1 Meteorological regimes

Figure 2 shows two distinct linear regimes for both sites' spectra in the value of the amplitude of the waves making up the LSP, which meet at around 10 days. Very similar spectra are seen in physical parameters in the atmosphere (Lovejoy and Schertzer, 2013a, b). There are 3 main scaling regimes of meteorological variability (Lovejoy and Schertzer, 2013a, b):
5   'weather', 'macroweather' and 'climate', with each regime being the outcome of different dynamical processes.

Weather processes range from microscale local turbulence to planetary scale weather systems, with the temporal lifetimes of these features roughly proportional to their spatial scale (Lovejoy and Schertzer, 2013b). The variability induced on O_3 also scales accordingly to these, thus the weather regime for O_3 is represented by a steep spectral gradient (on the log-log spectrum - Fig. 2) from 2 hours to ~10 days, after which there is a sharp transition to a flatter gradient. The change in the gradient at
10   around 10 days is physically caused by the finite size of the Earth giving a limit to the lifetime of the biggest planetary scale weather systems. After ~10 days the flat spectral gradient is a result of being the average of the largest planetary scale weather systems, being no more than low-frequency weather, with no new dynamical elements or forcing mechanism, the statistics of this regime being well captured by unforced 'control' runs of General Circulation Models (Lovejoy and Schertzer, 2013a). The regime has been shown for metrological spectra to extend out to 10-100 years, and is termed 'macroweather' (Lovejoy and
15   Schertzer, 2013b). The final regime is characterised by a steep increase from the flat macroweather gradient between 10-100 years caused by new (internal) low-frequency nonlinear interactions or (external) solar, volcanic or anthropogenic forcings, and represents long term changes of the macroweather. Human induced changes would be termed 'climate change'. As our work only uses time series of 5 years in length we do not see evidence of any climate regime for our spectra. We thus we end up with 2 regimes to describe the impact of meteorology on surface O_3 variability: weather (2 hours - 10 days) and macroweather (>
20   10 days).

These regimes can be described by fitting a model of two joint piecewise linear functions in log-log space to the spectrum (minimising the residuals). We set the transition point at 10 days, as the theoretical maximum lifetime for the largest planetary scale weather systems (Lovejoy and Schertzer, 2013b). We only use periods less than 100 days, for the few points beyond this value are noisy and can often introduce significant variability into this fitting. The upper panels of Fig. 2 show the linear fits
25   (green line) to the observed surface O_3 spectra for both Cape Verde and Lompoc.

To find periods which deviate from these fits, we scale the fitted models by percentiles of the Chi-Squared probability distribution to obtain false-alarm levels (Schulz and Mudelsee, 2002). Peaks exceeding these false-alarm levels indicate non-model components in the time series, and should be considered significant (Schulz and Mudelsee, 2002). Here, we take frequencies that have an amplitude above the 99th percent confidence level to be significant. Our attention now focuses on these significant
30   frequencies, namely the annual and daily peaks (and their harmonics).

3.2 Annual and daily cycles

From Fig. 2 it is evident that there are significant peaks on annual and daily timescales for both Cape Verde and Lompoc. There are also additional significant harmonic peaks ($\frac{1}{2}$ daily for Cape Verde; $\frac{1}{2}$, $\frac{1}{3}$, $\frac{1}{4}$, $\frac{1}{5}$, $\frac{1}{6}$, $\frac{1}{7}$, $\frac{1}{8}$, $\frac{1}{9}$, $\frac{1}{10}$, $\frac{1}{11}$, $\frac{1}{12}$ daily and $\frac{1}{2}$ annual

for Lompoc). These periodic cycles are driven by the planetary processes of the Earth's rotation around its own axis and its rotation around the sun both of which changes the predominant driving force for the atmosphere, solar radiation. Variability in solar radiation is not sinusoidal in nature, and the atmosphere is not linear in its response. Thus any harmonics are a product of the non-sinusoidal shape of the daily and annual cycles of ozone (Valenzuela and Pontt, 2009). Parrish et al. (2016) finds

5 that the annual and half-annual cycles are enough to characterise the seasonal variability of marine boundary layer O_3, and that the forcing responsible for the half-annual cycle a-priori is attributable to the 2nd harmonic of the photolysis rate of O_3. It is important to note however, that the the harmonics do not have to have independent physical forcings. The power of the harmonics can simply be a function of the mathematics.

For the surface ozone observational dataset described in Sect. 4 (Sofen et al., 2016) we find almost all sites show significant

10 peaks at the fundamentals (and most harmonics) of the annual and daily timescales. It is notable that we do not find any sites that show significance of a 7 day cycle (Altshuler et al., 1995; Marr and Harley, 2002; Beirle et al., 2003). Application of this approach to longer time series may also allow the investigation of other characteristic timescales such as NAO or ENSO (Ziemke et al., 2015).

3.2.1 Definition of 'seasonal' and 'diurnal' cycles

15 For all of the sites investigated the amplitude of the daily cycle is always significantly larger than any of its harmonics. However, this is not true for the annual cycle, as the magnitude of the half-annual cycle can sometimes compete with that of the annual cycle. To bring together the fundamental and the harmonics we superpose the fundamental and the harmonic signals to create 'seasonal' and 'diurnal' cycles. We show an example of this in Fig. 3, where the average, 1st (fundamental), 2nd, 3rd and 4th harmonics are superposed to create the net waveform. We choose to superpose down to the 12th harmonic for the diurnal cycle,

20 and 4th harmonic for the seasonal cycle as they are the highest harmonics for each periodicity that we find significance (> 99th percent confidence level). We characterise the superposed cycles with their amplitude being half the peak to trough height and their phase being the timing of the maxima. We modify the LSP code to ensure we estimate precisely at 1 day (and 2nd to 12th harmonics) and 365.25 days (and 2nd, 3rd and 4th harmonics) to ensure accurate estimation of these cycles. From this point onwards all references to the 'seasonal' or 'diurnal' cycle refer to the superposition of the respective fundamental and

25 harmonics, and any 'annual' and 'daily' references refer to solely the fundamental terms.

3.2.2 Fraction of total variance associated with a periodicity

The significance of the diurnal or seasonal cycles varies by location. We can calculate the fractional variance (σ^2) that both periodic waveforms contribute to the raw time series variance. We calculate this by extending both periodic waveforms to be the span of the raw time series, and take the fraction of the σ^2 of each waveform to the time series σ^2. Going further, superposing

30 the extended diurnal and seasonal waveforms gives a periodic waveform representative of the total periodic σ^2. In the same way as previous, we take the fraction of the total periodic σ^2 to the time series σ^2. Removing the total periodic waveform (including gaps) from the raw time series gives a time series which is solely derived of the weather and macroweather 'noise'.

The variances of these periodic and noise time series are essentially additive so that $\sigma^2(\text{diurnal}) + \sigma^2(\text{seasonal}) + \sigma^2(\text{noise}) = \sigma^2(\text{timeseries})$.

4 Application to observations

We apply these methods to an updated hourly version of the long-term surface ozone dataset from Sofen et al. (2016), compiled for the task of model evaluation. The dataset applies multiple stringent data quality checks: removing urban sites, duplicate sites, coarse and partial year data and obvious outliers. The data is originally drawn from the AirBase, CAPMON, CASTNET, EANET, EMEP, EPA AQS, NAPS, SEARCH and WMO GAW monitoring networks (see Sofen et al. (2016) and references therein for details), and for simplicity we choose the period between 2005 and 2010 as this represents the most comprehensively observed time period. We exclude sites with data gaps of more than 365 days in this period and additionally sites with data gaps greater than 60 days in 3 or more years. We additionally limit the sites to be below 1.5km from sea-level. Figure 4 shows the location of the 710 valid sites. Most of the sites are from the US EPA AQS and EU AirBase datasets which leads to an over representation of northern continental mid-latitude locations and an under representation of other areas of world.

We now investigate these observations in the context of the Lomb-Scargle derived diurnal and seasonal cycles.

4.1 Significance of seasonal and diurnal cycle

Figure 5 shows the fraction of the variance at each site that is explained by the seasonal, diurnal and the combined total periodic waveform. For most locations the seasonal cycle represents a much larger fractional variance than the diurnal cycle.

The greatest contribution to total variance from the seasonal cycle is for the Antarctic site (85%) and the oceanic and continental Southern Hemisphere (SH) sites (30-60%). This reflects the lack of anthropogenic influence and spatial homogeneity of these regions leading to small spatial gradients in O_3. Without spatial gradients to advect, weather systems cannot induce much variability, thus diurnal and seasonal variability dominates. For high NO_X regions in the North Eastern US, Southern and Central Europe and Japan (Fig. 13c), the seasonal cycle contributes 30-50% of the total variance. In Southern Central US contribution from the seasonal cycle to the total variability is very small (2-10%).

For the oceanic, polar and sites in low NO_X areas in the extra-tropics (i.e. Cape Point (34.21° S, 18.29° E) - the most south-westerly point of Africa) the diurnal cycle is negligible. These diurnal cycles are typically small as ozone production and loss in these low NO_X environments is small. However, it is a major contributor (20-40%) to the total variability for some low latitude regions in North America and Europe where high NO_X concentrations and photolysis rates lead to significant diurnal cycles.

Superposition of the diurnal and seasonal cycles gives a measure of the fraction of total variance induced from periodicity. For most sites the percentage contribution is between 40 and 60%. The highest value being for the Antarctic site (85%). The site with the lowest % contribution from periodicity is in Indonesia (15%), almost on the equator, where there is very little variability in the solar radiation.

From this analysis it is evident that forcing of the atmosphere from seasonal and diurnal processes (changes in solar irradiation, chemistry, emissions etc.) are for responsible for the most part for around 50% of the variability seen in these sites. The remaining 50% of the variability is attributable to changes on the weather or macroweather timescales due to processes such as boundary layer mixing, synoptic systems, changing emissions etc. We now describe in more detail the seasonal and diurnal cycles seen at different locations.

4.2 Seasonal cycle

The seasonal cycle of ozone has been subject to much discussion (Derwent and Davies, 1994; Logan, 1985; Monks et al., 2000; Monks, 2000; Tanimoto et al., 2005; Cooper et al., 2010, 2014; Carpenter et al., 2010; Parrish et al., 2013; Clifton et al., 2014; Parrish et al., 2016). In general, NH mid-latitude continental sites in the late 2000's show a springtime maxima, which has shifted from a broad summertime peak in the 1990's (Cooper et al., 2014). This change is strongly associated with NOx emission reductions in Europe and North America due to air quality legislation (Parrish et al., 2013; Clifton et al., 2014), however some of the most polluted urban sites still show a summertime peak (Cooper et al., 2014). Extra-tropical baseline sites show a consistent winter-spring maxima and tropical baseline sites a small winter maxima.

Our findings are consistent with the literature. The upper panels of Fig. 6 show the amplitude of the seasonal waveform for the observations. In general, most amplitudes are in the range of 5-15 ppbv. Sites influenced by highly polluted outflow such as the Central Valley in the US and the Po Valley in Italy show large amplitudes (up to 22 ppbv). High amplitudes can also be seen in the Asian sites downwind of China, particularly to the south of Japan (up to 23 ppbv).

The maxima in the observed seasonal waveforms (upper panels of Fig. 7) occurs in the spring (April, May) for most of the continental sites with a tendency for later peaks in Southern Europe. The small number of continental sites in the Southern Hemisphere (SH) show peaks 3-6 months out of phase compared to the Northern Hemisphere (NH), peaking in the SH late-winter to spring (August - October). The SH oceanic site, American Samoa (14.27° S, 170.13° W), has a winter phase (July), whereas the two NH oceanic sites have springtime phases (March and April). This is suggestive that the lower pollution associated with the SH sites generally leads to an earlier seasonal peak in O_3.

4.3 Diurnal cycle

The upper panels of Fig. 8 show the observational amplitudes of the diurnal cycle. In most of the locations this is in the range of 0-15 ppbv, with a tendency for larger amplitudes towards the tropics where solar radiation is more intense. There are also higher amplitudes in regions with higher NO_X emissions (Fig. 13c), with again the Central and Po Valleys being evident.

Significant differences between sites can be seen in the phases of the diurnal cycle (upper panels of Fig. 9). Baseline sites (i.e. American Samoa) show a phase which peaks close to dawn, reflecting photochemical O_3 destruction during the day and O_3 build up at night. Continental sites (i.e. Lompoc) show maxima in the early afternoon due to photochemical ozone production during the day.

The amplitude and phase of the diurnal and seasonal waveforms give a compact method of summarising much of the variability seen in surface ozone sites. We now explore how a Chemistry Transport Model (CTM) simulates these observations.

5 Model perspective

GEOS-Chem is a global 3-D CTM driven by assimilated meteorological observations from the Goddard Earth Observing System (GEOS) of the NASA Global Modelling Assimilation Office (GMAO). The basic model is described in (Bey et al., 2001). We run version v9.01.03, using GEOS5 analysed meteorology at $2°x2.5°$ resolution run for 5 years between 2005 and 2010, outputting surface hourly O_3 in each gridbox. Global anthropogenic emissions of CO, NO_X, and SO_2 are from the global EDGAR v3.2 inventory (Olivier et al., 2005). Global anthropogenic emissions of Non-Methane VOCs (NMVOCs) are from the RETRO monthly global inventory for the year 2000, as described by Hu et al. (2015), except for ethane (Xiao et al., 2008) and global biofuel emissions (Yevich and Logan, 2003). Inventories are scaled for individual years on the basis of economic data. Regional inventories are used in certain regions where there is improved information, as described by van Donkelaar et al. (2008). There are also inputs of NO_X from additional sources i.e. aircraft (Wang et al., 1998), ships (Vinken et al., 2011) and biomass burning (Giglio et al., 2010). Inputs from lightning and soil NO_X are calculated online (Yienger and Levy, 1995; Murray et al., 2012). Biogenic VOC emissions are from the global MEGAN v2.1 inventory (also calculated online) (Guenther et al., 2006). Stratosphere/troposphere exchange is handled as a parameterised climatological representation of species sources and sinks, (McLinden et al., 2000; Murray et al., 2012). Boundary layer mixing is parameterised using a non-local scheme which considers different states of mixing within the boundary layer as determined by the static instability (Holtslag and Boville, 1993; Lin and McElroy, 2010).

5.1 Modelled power spectrum

The power spectra for the modelled surface O_3 at Cape Verde and Lompoc are shown in the lower panels of Fig. 2. As for the observed spectra the weather and macroweather regimes are visibly separated at around 10 days. The model underestimates the amplitude on the shortest timescales for both sites (< 3 days). This is unsurprising given the model spatial scale ($2°x2.5°$, approx. 250km) and the timescale for model meteorological field updates (3 or 6 hours). As the timescale increases, the power in the model increases until it is comparable to that observed. This occurs at roughly 3 days. After this point the model appears to well simulate the power spectrum for both the weather and macroweather regimes. Thus care needs to be taken in interpreting output of this model on timescales of less than around 3 days as much of the meteorological variability will be missing. In general this will be true for all models. Therefore, on some timescales the model cannot be expected to interpret the observed variability, and this limitation should be considered when preparing model experiments.

As with the observations there are peaks at 365.25 days and 1 day with appropriate harmonics. As per the observations we superpose the daily and annual fundamentals with their harmonics to produce seasonal and diurnal signals which we describe with a phase and amplitude. We now investigate the amplitude and phase of the modelled diurnal and seasonal cycles.

5.2 Seasonal cycle

The lowest panel of Fig. 6 shows the modelled amplitude for the seasonal cycle in surface ozone. As with the observations, the model shows large amplitudes over regions with significant anthropogenic NO_X emissions (Fig. 13c) such as North America,

Europe and Asia (up to 26 ppbv). Regions with significant seasonal cycles in the NO_X emissions, such as from biomass burning in the Amazon and Central Africa also have large cycles (up to 27 ppbv). These large amplitudes can be seen to extend away from the source regions into the Pacific and Indian oceans. Over the remote tropical oceans the seasonal cycle is very small (1 ppbv). Due to a scarcity of observations, many of these features are unobserved.

5   Figure 7 shows the global seasonal phase of modelled surface O_3 (lower panel). There are distinct bands of phases. Over polluted NH continental regions a July-September maximum is calculated, with the cleaner northern extra-tropics showing a April-May maximum and the clean tropics a December-February maximum. In the SH there is a September-December maximum for continental regions, and a July-September maximum over the oceans and Antarctica.

5.3   Diurnal cycle

10   The largest diurnal amplitudes (lower panel of Fig. 8) are found in Eastern China (up to 28 ppbv) where the emissions of NO_X are greatest. This leads to large diurnal photochemical production of O_3 but also large titration by NO at night. High diurnal amplitudes are also found over the polluted North East US (13-17 ppbv), Central Europe (10-13 ppbv) and India (11-15 ppbv). Again, regions with significant seasonal cycles in the NO_X emissions from biomass burning also have large amplitudes i.e. Amazon, Indonesia and Central Africa.

15   Figure 9 shows the global diurnal phases of modelled surface O_3 (lower panel). As with the observations the 2 distinct clean and polluted regimes emerge. The polluted areas almost all have diurnal cycle peaking at 14:00 or 15:00. This band includes all continental regions (except Greenland and polar regions). It also includes a band across the Northern Pacific and Northern Atlantic Oceans. The clean areas almost all have a phase at 08:00, the exception being a circumpolar band of phases which peak at 04:00 around Antarctica. The diurnal phase at the poles looks incoherent, which is predominantly due to the very small 20   amplitudes in these regions, thus the phase becomes practically irrelevant.

6   Model - Measurement comparisons

The previous sections investigate the absolute amplitude and phase of the seasonal and diurnal cycle. In this section we use these parameters to investigate model performance against observations.

6.1   Seasonal cycle

25   Figure 10 shows the polar representation of the seasonal cycle for the observations, model and the difference between the two. North American and European site seasonal amplitudes are on average overestimated, (up to 16 ppbv). The seasonal phase also shows biases with most sites' phases in North America and Europe peaking 1-5 months later than the observations, in mid-late summer rather than mid-late spring. Seasonal amplitudes for the African, Antarctic, Arctic, Asian, Oceania and oceanic sites are all underestimated (up to 10 ppbv) but their phases show generally good agreement with the observations.

30   Figure 11 shows the spatial distribution of the difference for the seasonal amplitudes and phases. The biggest model over-estimations for the amplitudes (upper panels) are in regions with high very O_3 precursors, i.e. North East US (up to 16 ppbv)

and mainland Central Europe (to to 11 ppbv); both generally at sites inland, away from oceanic influence. In contrast, it is the coastal and oceanic sites where the model underestimations are greatest, with the largest coming in Asia (5-10 ppbv) and Eastern Canada (up to 8 ppbv).

The lower panels of Fig. 11 show in mainland Europe the seasonal phases are generally 1-3 months too late in the model and 2-4 months too late in the North East/South East US. The biggest phase differences come in the Central South US with the model phases approximately 4-5 months too late (a region where the seasonal cycle contributes very little to the total variance, Fig. 5).

6.2 Diurnal cycle

Figure 10 also shows the polar representation of the diurnal cycle observations, model and difference. The model has some skill in determining the diurnal amplitudes. There is on average an overestimation of North American, European and Asian diurnal amplitudes (up to 17 ppbv). Amplitudes for the clean oceanic sites are well estimated, with the rest of the sites in Oceania, Africa, Antarctic and Arctic displaying reasonable agreement. The model has generally good skill for simulating the diurnal phases (ignoring the polar sites), however notable biases show in the oceanic and Asian sites with the model up to 5 hours late, and up 4 hours early respectively for the groupings. Additionally for the North American and European groupings, the model simulates the vast majority of phases in a narrow band, where there is a broader grouping of phases in the observations. This may represent issues with the timing of processes such as boundary layer mixing which is suggested to be excessive (Travis et al., 2016).

Spatially, Fig. 12 upper panels, the biggest overestimations in the amplitudes are again in regions with high emissions of O_3 precursors: Central Valley US (up to 17 ppbv), North East US (up to 14 ppbv), Japan (up to 11 ppbv) and mainland Central Europe (up to 11 ppbv). The biggest underestimations come in coastal regions i.e. West Coast US (up to 11 ppbv) and Southern Europe (up to 10 ppbv).

The lower panels of Fig. 12 show the model in the high NO_X emitting regions of North East US and Central Europe to have too early a phase also (- 1-2 hours). The largest phase offsets (excluding polar sites) are found in the oceanic sites of Bermuda and American Samoa (+3 and +5 hours).

6.3 Possible causes of biases

A range of model biases are evident in this analysis. These may be explained by a range of model errors/uncertainties in the emissions, deposition, chemistry, photolysis rates, boundary layer mixing, stratospheric transport, tropospheric transport, resolution etc.

The most discussed uncertainties lie in the emissions. Probably the most accurate emission estimates are for North America and Europe, but even here significant uncertainties exist. Anderson et al. (2014) finds the anthropogenic US National Emissions Inventory (NEI) 2005 NO_X emissions (projected to 2011) in the Mid-East US to be 51-70% too high compared with measurements taken on the DISCOVER-AQ field campaign. The NEI 2011 emissions appear to overestimated by an even larger margin. Vestreng et al. (2009) finds ±8-25% uncertainties in European NO_X emissions. Stein et al. (2014) also recently

found wintertime systematic underestimates in NH CO by a global CTM, best offset by increases in winter CO road traffic emissions together with an improved CO dry deposition scheme.

As anthropogenic NO_X decreases, the relative importance of lightning and soil NO_X is much greater and the importance of low-NO_X isoprene chemistry increases (Palmer, 2003; Fiore et al., 2014). Millet et al. (2008) show the MEGAN v2.1 biogenic emission inventory in the US (Guenther et al., 2006) overestimates emissions of isoprene in areas where it specifies high emission factors.

Reduced winter/early-spring photochemical removal by NO titration (Jonson et al., 2006); efficient transport of enhanced springtime O_3 from East Asia (Wild and Akimoto, 2001; Tanimoto, 2002; Tanimoto et al., 2005); as well as earlier peak stratospheric-tropospheric exchange to the surface, may be synergistic factors along with reduced emissions in bringing about a springtime ozone maximum for NH mid-latitude continental sites (Parrish et al., 2013).

We attempt to correlate seasonal model O_3 amplitude and phase biases with average 2005-2010 model NO_X, Fig. 13. For the seasonal cycle the greatest overestimates of the amplitude generally correlate with the highest NO_X concentrations in the model (panel a), however this is not true for the largest biases in the phase (panel b). Although the phase biases are not linear with NO_X emissions, from the amplitude biases it is clear that evaluation of NO_X emissions would be a sensible place to start in trying to correct biases.

7 Conclusions

We have used a Lomb-Scargle methodology to spectrally analyse surface ozone. We find spectra with distinct relationships between amplitude and period due to meteorological processes (weather and macroweather) as well as peaks at 1 and 365.25 day timescales (and harmonics). The amplitude and phase of the periodicity associated with these timescales varies significantly between sites.

A comparison between model output and measured surface ozone spectra shows a model underestimate of the amplitudes at high frequencies due the spatial and temporal scales inherent in the model.

A comparison between of the periodic components for model and measurements shows model biases in the seasonal cycle in the mid-latitude NH, where there is a general overestimate of the seasonal amplitudes in North America and Europe of up to 16 ppbv, together with delayed phase maxima by 1-5 months. We show the amplitude biases may be related to errors in the emissions of NO_X. We find lower biases for the diurnal cycle but show the majority of amplitudes in Europe and North America to be overestimated, by up to 17ppbv.

This methodology has significant scope for future use. It can be applied to a range of model-measurement applications and the associated metrics are highly suitable for Multimodel Intercomparison Projects (MIPs). We aim to apply this methodology to the ACCMIP and CCMI MIPs to explore differences in chemistry between the different CTM/ESMs.

Acknowledgements. This work was funded by the NERC BACCHUS and CAST projects NE/L01291X/1, NE/J006165/1. Thanks go to the data providers at the AirBase, CAPMON, CASTNET, EANET, EMEP, EPA AQS, NAPS, SEARCH and WMO GAW monitoring networks

for the data to make this evaluation possible. Thanks also go to colleagues at the Wolfson Atmospheric Chemistry Laboratories, University of York for the maintaining of the monitoring station in Cape Verde, providing data for this paper.

References

Altshuler, S., Arcado, T., and Lawson, D.: Weekday vs weekend ambient ozone concentrations - discussion and hypotheses with focus on northern California, J. Air Waste Manage. Assoc., 45, 967–972, doi:10.1080/10473289.1995.10467428, 1995.

Anderson, D. C., Loughner, C. P., Diskin, G., Weinheimer, A., Canty, T. P., Salawitch, R. J., Worden, H. M., Fried, A., Mikoviny, T., Wisthaler, A., and Dickerson, R. R.: Measured and modeled CO and NOy in DISCOVER-AQ: An evaluation of emissions and chemistry over the eastern US, Atmos. Environ., 96, 78–87, doi:10.1016/j.atmosenv.2014.07.004, 2014.

Beirle, S., Platt, U., Wenig, M., and Wagner, T.: Weekly cycle of NO2 by GOME measurements: a signature of anthropogenic sources, Atmos. Chem. Phys., 3, 2225–2232, doi:10.5194/acp-3-2225-2003, 2003.

Bey, I., Jacob, D. J., Yantosca, R. M., Logan, J. A., Field, B. D., Fiore, A. M., Li, Q. B., Liu, H. G. Y., Mickley, L. J., and Schultz, M. G.: Global modeling of tropospheric chemistry with assimilated meteorology: Model description and evaluation, J. Geophys. Res. Atmos., 106, 23 073–23 095, doi:10.1029/2001jd000807, 2001.

Carpenter, L. J., Fleming, Z. L., Read, K. A., Lee, J. D., Moller, S. J., Hopkins, J. R., Purvis, R. M., Lewis, A. C., Muller, K., Heinold, B., Herrmann, H., Fomba, K. W., van Pinxteren, D., Muller, C., Tegen, I., Wiedensohler, A., Muller, T., Niedermeier, N., Achterberg, E. P., Patey, M. D., Kozlova, E. A., Heimann, M., Heard, D. E., Plane, J. M. C., Mahajan, A., Oetjen, H., Ingham, T., Stone, D., Whalley, L. K., Evans, M. J., Pilling, M. J., Leigh, R. J., Monks, P. S., Karunaharan, A., Vaughan, S., Arnold, S. R., Tschritter, J., Pohler, D., Friess, U., Holla, R., Mendes, L. M., Lopez, H., Faria, B., Manning, A. J., and Wallace, D. W. R.: Seasonal characteristics of tropical marine boundary layer air measured at the Cape Verde Atmospheric Observatory, J. Atmos. Chem., 67, 87–140, doi:10.1007/s10874-011-9206-1, 2010.

Clifton, O. E., Fiore, A. M., Correa, G., Horowitz, L. W., and Naik, V.: Twenty-first century reversal of the surface ozone seasonal cycle over the northeastern United States, Geophys. Res. Lett., 41, 7343–7350, doi:10.1002/2014GL061378, 2014.

Cooper, O. R., Parrish, D. D., Stohl, A., Trainer, M., Nédélec, P., Thouret, V., Cammas, J. P., Oltmans, S. J., Johnson, B. J., Tarasick, D., Leblanc, T., McDermid, I. S., Jaffe, D., Gao, R., Stith, J., Ryerson, T., Aikin, K., Campos, T., Weinheimer, A., and Avery, M. A.: Increasing springtime ozone mixing ratios in the free troposphere over western North America., Nature, 463, 344–348, doi:10.1038/nature08708, 2010.

Cooper, O. R., Gao, R.-S., Tarasick, D., Leblanc, T., and Sweeney, C.: Long-term ozone trends at rural ozone monitoring sites across the United States, 1990-2010, J. Geophys. Res. Atmos., 117, D22 307, doi:10.1029/2012JD018261, 2012.

Cooper, O. R., Parrish, D. D., Ziemke, J., Balashov, N. V., Cupeiro, M., Galbally, I. E., Gilge, S., Horowitz, L., Jensen, N. R., Lamarque, J.-F., Naik, V., Oltmans, S. J., Schwab, J., Shindell, D. T., Thompson, A. M., Thouret, V., Wang, Y., and Zbinden, R. M.: Global distribution and trends of tropospheric ozone: An observation-based review, Elem. Sci. Anthr., 2, 000 029, doi:10.12952/journal.elementa.000029, 2014.

Derwent, R. and Davies, T.: Modelling the impact of NOx or hydrocarbon control on photochemical ozone in Europe, Atmos. Environ., 28, 2039–2052, doi:10.1016/1352-2310(94)90472-3, 1994.

Derwent, R., Stevenson, D., Doherty, R., Collins, W., and Sanderson, M.: How is surface ozone in Europe linked to Asian and North American NOx emissions?, Atmos. Environ., 42, 7412–7422, doi:10.1016/j.atmosenv.2008.06.037, 2008.

Dutton, S. J., Rajagopalan, B., Vedal, S., and Hannigan, M. P.: Temporal patterns in daily measurements of inorganic and organic speciated PM2.5 in Denver., Atmos. Environ. (1994)., 44, 987–998, doi:10.1016/j.atmosenv.2009.06.006, 2010.

Ehhalt, D. H.: Photooxidation of trace gases in the troposphere, Phys. Chem. Chem. Phys., 1, 5401–5408, doi:10.1039/a905097c, 1999.

Fiore, A., Oberman, J., Lin, M., Zhang, L., Clifton, O., Jacob, D., Naik, V., Horowitz, L., Pinto, J., and Milly, G.: Estimating North American background ozone in U.S. surface air with two independent global models: Variability, uncertainties, and recommendations, Atmos. Environ., 96, 284–300, doi:10.1016/j.atmosenv.2014.07.045, 2014.

Forster, P., Ramaswamy, V., Artaxo, P., Berntsen, T., Betts, R., Fahey, D. W., Haywood, J., Lean, J., Lowe, D. C., Myhre, G., Nganga, J., Prinn, R., Raga, G., Schulz, M., and Dorland, R. V.: Changes in Atmospheric Constituents and in Radiative Forcing, in: Climate Change 2007: The Physical Science Basis. Contribution of Working Group I to the Fourth Assessment Report of the Intergovernmental Panel on Climate Change, edited by Solomon, S., Qin, D., Manning, M., Chen, Z., Marquis, M., Averyt, K., Tignor, M., and Miller, H., pp. 131–215, Cambridge University Press, Cambridge, U.K, 2007.

Fowler, D., Pilegaard, K., Sutton, M., Ambus, P., Raivonen, M., Duyzer, J., Simpson, D., Fagerli, H., Fuzzi, S., Schjoerring, J., Granier, C., Neftel, A., Isaksen, I., Laj, P., Maione, M., Monks, P., Burkhardt, J., Daemmgen, U., Neirynck, J., Personne, E., Wichink-Kruit, R., Butterbach-Bahl, K., Flechard, C., Tuovinen, J., Coyle, M., Gerosa, G., Loubet, B., Altimir, N., Gruenhage, L., Ammann, C., Cieslik, S., Paoletti, E., Mikkelsen, T., Ro-Poulsen, H., Cellier, P., Cape, J., Horváth, L., Loreto, F., Niinemets, Ü., Palmer, P., Rinne, J., Misztal, P., Nemitz, E., Nilsson, D., Pryor, S., Gallagher, M., Vesala, T., Skiba, U., Brüggemann, N., Zechmeister-Boltenstern, S., Williams, J., O'Dowd, C., Facchini, M., de Leeuw, G., Flossman, A., Chaumerliac, N., and Erisman, J.: Atmospheric composition change: Ecosystems–Atmosphere interactions, Atmos. Environ., 43, 5193–5267, doi:10.1016/j.atmosenv.2009.07.068, 2009.

Giglio, L., Randerson, J. T., van der Werf, G. R., Kasibhatla, P. S., Collatz, G. J., Morton, D. C., and DeFries, R. S.: Assessing variability and long-term trends in burned area by merging multiple satellite fire products, Biogeosciences, 7, 1171–1186, doi:10.5194/bg-7-1171-2010, 2010.

Guenther, A., Karl, T., Harley, P., Wiedinmyer, C., Palmer, P. I., and Geron, C.: Estimates of global terrestrial isoprene emissions using MEGAN (Model of Emissions of Gases and Aerosols from Nature), Atmos. Chem. Phys., 6, 3181–3210, doi:10.5194/acp-6-3181-2006, 2006.

Harris, F.: On the use of windows for harmonic analysis with the discrete Fourier transform, in: Proc. IEEE, vol. 66, pp. 51–83, Institute of Electrical and Electronics Engineers (IEEE), doi:10.1109/PROC.1978.10837, 1978.

Hess, P. G. and Zbinden, R.: Stratospheric impact on tropospheric ozone variability and trends: 1990–2009, Atmos. Chem. Phys., 13, 649–674, doi:10.5194/acp-13-649-2013, 2013.

Hocke, K.: Phase estimation with the Lomb-Scargle periodogram method, Ann. Geophys. Hydrospheres Sp. Sci., 16, 356–358, http://www.ann-geophys.net/16/356/1998/., 1998.

Holtslag, A. A. M. and Boville, B. A.: Local versus nonlocal boundary layer diffusion in a global climate model, J. Clim., 6, 1825–1842, doi:10.1175/1520-0442(1993)006<1825:LVNBLD>2.0.CO;2, 1993.

Horne, J. H. and Baliunas, S. L.: A prescription for period analysis of unevenly sampled time-series, Astrophys. J., 302, 757–763, doi:10.1086/164037, 1986.

Hu, L., Millet, D. B., Baasandorj, M., Griffis, T. J., Travis, K. R., Tessum, C. W., Marshall, J. D., Reinhart, W. F., Mikoviny, T., Müller, M., Wisthaler, A., Graus, M., Warneke, C., and de Gouw, J.: Emissions of C 6 -C 8 aromatic compounds in the United States: Constraints from tall tower and aircraft measurements, J. Geophys. Res. Atmos., 120, 826–842, doi:10.1002/2014JD022627, 2015.

Jenkin, M. E. and Clemitshaw, K. C.: Ozone and other secondary photochemical pollutants: chemical processes governing their formation in the planetary boundary layer, Atmos. Environ., 34, 2499–2527, doi:10.1016/S1352-2310(99)00478-1, 2000.

Jonson, J., Simpson, D., Fagerli, H., and Solberg, S.: Can we explain the trends in European ozone levels?, Atmos. Chem. Phys., 6, 51–66, doi:10.5194/acp-6-51-2006, 2006.

Levy, H.: Photochemistry of the lower troposphere, Planet. Space Sci., 20, 919–935, doi:10.1016/0032-0633(72)90177-8, 1972.

Lin, J.-T. and McElroy, M. B.: Impacts of boundary layer mixing on pollutant vertical profiles in the lower troposphere: Implications to satellite remote sensing, Atmos. Environ., 44, 1726–1739, doi:10.1016/j.atmosenv.2010.02.009, 2010.

Logan, J. A.: Tropospheric ozone: Seasonal behavior, trends, and anthropogenic influence, J. Geophys. Res., 90, 10 463, doi:10.1029/JD090iD06p10463, 1985.

Logan, J. A., Staehelin, J., Megretskaia, I. A., Cammas, J.-P., Thouret, V., Claude, H., De Backer, H., Steinbacher, M., Scheel, H.-E., Stübi, R., Fröhlich, M., and Derwent, R.: Changes in ozone over Europe: Analysis of ozone measurements from sondes, regular aircraft (MOZAIC) and alpine surface sites, J. Geophys. Res., 117, D09 301, doi:10.1029/2011JD016952, 2012.

Lomb, N. R.: Least-squares frequency-analysis of unequally spaced data, Astrophys. Space Sci., 39, 447–462, doi:10.1007/bf00648343, 1976.

Lovejoy, S. and Schertzer, D.: Low-Frequency Weather and the Emergence of the Climate, in: Extrem. Events Nat. Hazards Complex. Perspect., pp. 231–254, American Geophysical Union, doi:10.1029/2011GM001087, 2013a.

Lovejoy, S. and Schertzer, D.: The Weather and Climate: Emergent Laws and Multifractal Cascades, Cambridge University Press, Cambridge, U.K, 2013b.

Marr, L. C. and Harley, R. A.: Spectral analysis of weekday–weekend differences in ambient ozone, nitrogen oxide, and non-methane hydrocarbon time series in California, Atmos. Environ., 36, 2327–2335, doi:10.1016/S1352-2310(02)00188-7, 2002.

McLinden, C. A., Olsen, S. C., Hannegan, B., Wild, O., Prather, M. J., and Sundet, J.: Stratospheric ozone in 3-D models: A simple chemistry and the cross-tropopause flux, J. Geophys. Res., 105, 14 653, doi:10.1029/2000JD900124, 2000.

Millet, D. B., Jacob, D. J., Boersma, K. F., Fu, T.-M., Kurosu, T. P., Chance, K., Heald, C. L., and Guenther, A.: Spatial distribution of isoprene emissions from North America derived from formaldehyde column measurements by the OMI satellite sensor, J. Geophys. Res., 113, D02 307, doi:10.1029/2007JD008950, 2008.

Monks, P. S.: A review of the observations and origins of the spring ozone maximum, Atmos. Environ., 34, 3545–3561, doi:10.1016/s1352-2310(00)00129-1, 2000.

Monks, P. S.: Gas-phase radical chemistry in the troposphere., Chem. Soc. Rev., 34, 376–95, doi:10.1039/b307982c, 2005.

Monks, P. S., Salisbury, G., Holland, G., Penkett, S. A., and Ayers, G. P.: A seasonal comparison of ozone photochemistry in the remote marine boundary layer, Atmos. Environ., 34, 2547–2561, doi:10.1016/S1352-2310(99)00504-X, 2000.

Monks, P. S., Archibald, A. T., Colette, A., Cooper, O., Coyle, M., Derwent, R., Fowler, D., Granier, C., Law, K. S., Mills, G. E., Stevenson, D. S., Tarasova, O., Thouret, V., von Schneidemesser, E., Sommariva, R., Wild, O., and Williams, M. L.: Tropospheric ozone and its precursors from the urban to the global scale from air quality to short-lived climate forcer, Atmos. Chem. Phys., 15, 8889–8973, doi:10.5194/acp-15-8889-2015, 2015.

Murray, L. T., Jacob, D. J., Logan, J. A., Hudman, R. C., and Koshak, W. J.: Optimized regional and interannual variability of lightning in a global chemical transport model constrained by LIS/OTD satellite data, J. Geophys. Res. Atmos., 117, D20 307, doi:10.1029/2012JD017934, 2012.

Musial, J. P., Verstraete, M. M., and Gobron, N.: Technical Note: Comparing the effectiveness of recent algorithms to fill and smooth incomplete and noisy time series, Atmos. Chem. Phys., 11, 7905–7923, doi:10.5194/acp-11-7905-2011, 2011.

Olivier, J., Aardenne, J.A, Dentener, F., Ganzeveld, L., and Peters, J.: Recent trends in global greenhouse gas emissions: regional trends and spatial distribution of key sources, Environmetal Sci., 2, doi:10.1080/15693430500400345, 2005.

Oltmans, S. J., Lefohn, A. S., Harris, J. M., Galbally, I., Scheel, H. E., Bodeker, G., Brunke, E., Claude, H., Tarasick, D., Johnson, B. J., Simmonds, P., Shadwick, D., Anlauf, K., Hayden, K., Schmidlin, F., Fujimoto, T., Akagi, K., Meyer, C., Nichol, S., Davies, J., Redondas, A., and Cuevas, E.: Long-term changes in tropospheric ozone, Atmos. Environ., 40, 3156–3173, doi:10.1016/j.atmosenv.2006.01.029, 2006.

5 Oltmans, S. J., Lefohn, A. S., Shadwick, D., Harris, J. M., Scheel, H. E., Galbally, I., Tarasick, D. W., Johnson, B. J., Brunke, E. G., Claude, H., Zeng, G., Nichol, S., Schmidlin, F., Davies, J., Cuevas, E., Redondas, A., Naoe, H., Nakano, T., and Kawasato, T.: Recent tropospheric ozone changes - A pattern dominated by slow or no growth, Atmos. Environ., 67, 331–351, doi:10.1016/j.atmosenv.2012.10.057, 2013.

Palmer, P. I.: Mapping isoprene emissions over North America using formaldehyde column observations from space, J. Geophys. Res., 108, 4180, doi:10.1029/2002JD002153, 2003.

10 Parrish, D. D., Law, K. S., Staehelin, J., Derwent, R., Cooper, O. R., Tanimoto, H., Volz-Thomas, A., Gilge, S., Scheel, H. E., Steinbacher, M., and Chan, E.: Lower tropospheric ozone at northern midlatitudes: Changing seasonal cycle, Geophys. Res. Lett., 40, 1631–1636, doi:10.1002/grl.50303, 2013.

Parrish, D. D., Lamarque, J.-F., Naik, V., Horowitz, L., Shindell, D. T., Staehelin, J., Derwent, R., Cooper, O. R., Tanimoto, H., Volz-Thomas, A., Gilge, S., Scheel, H.-E., Steinbacher, M., and Fröhlich, M.: Long-term changes in lower tropospheric baseline ozone con-
15 centrations: Comparing chemistry-climate models and observations at northern midlatitudes, J. Geophys. Res. Atmos., 119, 5719–5736, doi:10.1002/2013JD021435, 2014.

Parrish, D. D., Galbally, I. E., Lamarque, J.-F., Naik, V., Horowitz, L., Shindell, D. T., Oltmans, S. J., Derwent, R., Tanimoto, H., Labuschagne, C., and Cupeiro, M.: Seasonal cycles of O 3 in the marine boundary layer: Observation and model simulation comparisons, J. Geophys. Res. Atmos., 121, 538–557, doi:10.1002/2015JD024101, 2016.

20 Press, W. H. and Rybicki, G. B.: Fast algorithm for spectral-analysis of unevenly sampled data, Astrophys. J., 338, 277–280, doi:10.1086/167197, 1989.

Press, W. H., Teukolsky, S. A., Vetterling, W. T., and Flannery, B. P.: Numerical Recipes in Fortran 77 - The Art Of Scientific Computing - Volume I, vol. 1, Cambridge University Press, doi:10.1016/0169-2607(87)90037-X, 1992.

Rehfeld, K., Marwan, N., Heitzig, J., and Kurths, J.: Comparison of correlation analysis techniques for irregularly sampled time series,
25 Nonlinear Process. Geophys., 18, 389–404, doi:10.5194/npg-18-389-2011, 2011.

Scargle, J. D.: Studies in astronomical time-series analysis .2. Statistical aspects of spectral-analysis of unevenly spaced data, Astrophys. J., 263, 835–853, doi:10.1086/160554, 1982.

Schnell, J. L., Prather, M. J., Josse, B., Naik, V., Horowitz, L. W., Cameron-Smith, P., Bergmann, D., Zeng, G., Plummer, D. A., Sudo, K., Nagashima, T., Shindell, D. T., Faluvegi, G., and Strode, S. A.: Use of North American and European air quality networks to evaluate
30 global chemistry–climate modeling of surface ozone, Atmos. Chem. Phys., 15, 10 581–10 596, doi:10.5194/acp-15-10581-2015, 2015.

Schulz, M. and Mudelsee, M.: REDFIT: estimating red-noise spectra directly from unevenly spaced paleoclimatic time series, Comput. Geosci., 28, 421–426, doi:10.1016/s0098-3004(01)00044-9, 2002.

Schulz, M. and Stattegger, K.: SPECTRUM: Spectral analysis of unevenly spaced paleoclimatic time series, Comput. Geosci., 23, 929–945, doi:10.1016/s0098-3004(97)00087-3, 1997.

35 Sofen, E. D., Bowdalo, D., Evans, M. J., Apadula, F., Bonasoni, P., Cupeiro, M., Ellul, R., Galbally, I. E., Girgzdiene, R., Luppo, S., Mimouni, M., Nahas, A. C., Saliba, M., and Tørseth, K.: Gridded global surface ozone metrics for atmospheric chemistry model evaluation, Earth Syst. Sci. Data, 8, 41–59, doi:10.5194/essd-8-41-2016, 2016.

Stefan, S., Necula, C., and Georgescu, F.: Analysis of long-range transport of particulate matters in connection with air circulation over Central and Eastern part of Europe, Phys. Chem. Earth, Parts A/B/C, 35, 523–529, doi:10.1016/j.pce.2009.12.008, 2010.

Stein, O., Schultz, M. G., Bouarar, I., Clark, H., Huijnen, V., Gaudel, A., George, M., and Clerbaux, C.: On the wintertime low bias of Northern Hemisphere carbon monoxide found in global model simulations, Atmos. Chem. Phys., 14, 9295–9316, doi:10.5194/acp-14-9295-2014, 2014.

Stevenson, D. S., Dentener, F. J., Schultz, M. G., Ellingsen, K., van Noije, T. P. C., Wild, O., Zeng, G., Amann, M., Atherton, C. S., Bell, N., Bergmann, D. J., Bey, I., Butler, T., Cofala, J., Collins, W. J., Derwent, R. G., Doherty, R. M., Drevet, J., Eskes, H. J., Fiore, A. M., Gauss, M., Hauglustaine, D. A., Horowitz, L. W., Isaksen, I. S. A., Krol, M. C., Lamarque, J.-F., Lawrence, M. G., Montanaro, V., Müller, J.-F., Pitari, G., Prather, M. J., Pyle, J. A., Rast, S., Rodriguez, J. M., Sanderson, M. G., Savage, N. H., Shindell, D. T., Strahan, S. E., Sudo, K., and Szopa, S.: Multimodel ensemble simulations of present-day and near-future tropospheric ozone, J. Geophys. Res., 111, D08 301, doi:10.1029/2005JD006338, 2006.

Tanimoto, H.: Seasonal cycles of ozone and oxidized nitrogen species in northeast Asia 2. A model analysis of the roles of chemistry and transport, J. Geophys. Res., 107, 4706, doi:10.1029/2001JD001497, 2002.

Tanimoto, H., Sawa, Y., Matsueda, H., Uno, I., Ohara, T., Yamaji, K., Kurokawa, J., and Yonemura, S.: Significant latitudinal gradient in the surface ozone spring maximum over East Asia, Geophys. Res. Lett., 32, L21 805, doi:10.1029/2005GL023514, 2005.

Travis, K. R., Jacob, D. J., Fisher, J. A., Kim, P. S., Marais, E. A., Zhu, L., Yu, K., Miller, C. C., Yantosca, R. M., Sulprizio, M. P., Thompson, A. M., Wennberg, P. O., Crounse, J. D., St. Clair, J. M., Cohen, R. C., Laugher, J. L., Dibb, J. E., Hall, S. R., Ullmann, K., Wolfe, G. M., Pollack, I. B., Peischl, J., Neuman, J. A., and Zhou, X.: NOx emissions, isoprene oxidation pathways, vertical mixing, and implications for surface ozone in the Southeast United States, Atmos. Chem. Phys. Discuss., pp. 1–32, doi:10.5194/acp-2016-110, 2016.

Valenzuela, J. and Pontt, J.: Real-Time Interharmonics Detection and Measurement Based on FFT Algorithm, in: Proc. Appl. Electron., pp. 259–264, Institute of Electrical and Electronics Engineers (IEEE), Pilsen, 2009.

van Donkelaar, A., Martin, R. V., Leaitch, W. R., Macdonald, A. M., Walker, T. W., Streets, D. G., Zhang, Q., Dunlea, E. J., Jimenez, J. L., Dibb, J. E., Huey, L. G., Weber, R., and Andreae, M. O.: Analysis of aircraft and satellite measurements from the Intercontinental Chemical Transport Experiment (INTEX-B) to quantify long-range transport of East Asian sulfur to Canada, Atmos. Chem. Phys., 8, 2999–3014, doi:10.5194/acp-8-2999-2008, 2008.

Vestreng, V., Ntziachristos, L., Semb, A., Reis, S., Isaksen, I. S. A., and Tarrasón, L.: Evolution of NOx emissions in Europe with focus on road transport control measures, Atmos. Chem. Phys., 9, 1503–1520, doi:10.5194/acp-9-1503-2009, 2009.

Vinken, G. C. M., Boersma, K. F., Jacob, D. J., and Meijer, E. W.: Accounting for non-linear chemistry of ship plumes in the GEOS-Chem global chemistry transport model, Atmos. Chem. Phys., 11, 11 707–11 722, doi:10.5194/acp-11-11707-2011, 2011.

Wang, Y., Jacob, D. J., and Logan, J. A.: Global simulation of tropospheric O3 -NOx -hydrocarbon chemistry: 1. Model formulation, J. Geophys. Res., 103, 10 713, doi:10.1029/98JD00158, 1998.

WHO: WHO Air quality guidelines for particulate matter, ozone, nitrogen dioxide and sulfur dioxide: Global update 2005, World Health Organization, Regional Office for Europe, 2005.

Wild, O. and Akimoto, H.: Intercontinental transport of ozone and its precursors in a three-dimensional global CTM, J. Geophys. Res. Atmos., 106, 27 729–27 744, doi:10.1029/2000jd000123, 2001.

Xiao, Y., Logan, J. A., Jacob, D. J., Hudman, R. C., Yantosca, R., and Blake, D. R.: Global budget of ethane and regional constraints on U.S. sources, J. Geophys. Res., 113, D21 306, doi:10.1029/2007JD009415, 2008.

Yevich, R. and Logan, J. A.: An assessment of biofuel use and burning of agricultural waste in the developing world, Global Biogeochem. Cycles, 17, 1095, doi:10.1029/2002GB001952, 2003.

Yienger, J. J. and Levy, H.: Empirical model of global soil-biogenic NOx emissions, J. Geophys. Res., 100, 11 447, doi:10.1029/95JD00370, 1995.

5   Ziemke, J. R., Douglass, A. R., Oman, L. D., Strahan, S. E., and Duncan, B. N.: Tropospheric ozone variability in the tropics from ENSO to MJO and shorter timescales, Atmos. Chem. Phys., 15, 8037–8049, doi:10.5194/acp-15-8037-2015, 2015.
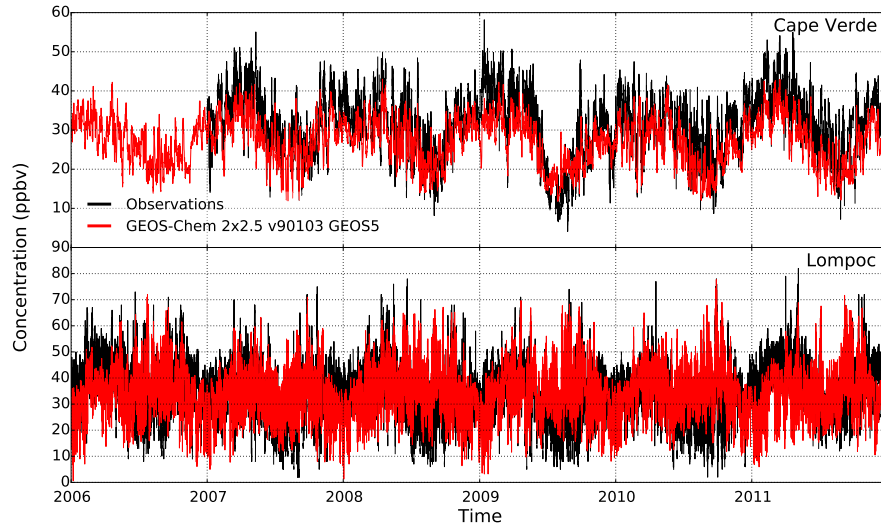
Figure 1. Time series of surface O$_3$ at Cape Verde (16.51° N, 24.52° W) and Lompoc (34.73° N, 120.43° W) for the observations (black) and the GEOS-Chem model (red), between 2006-2012.
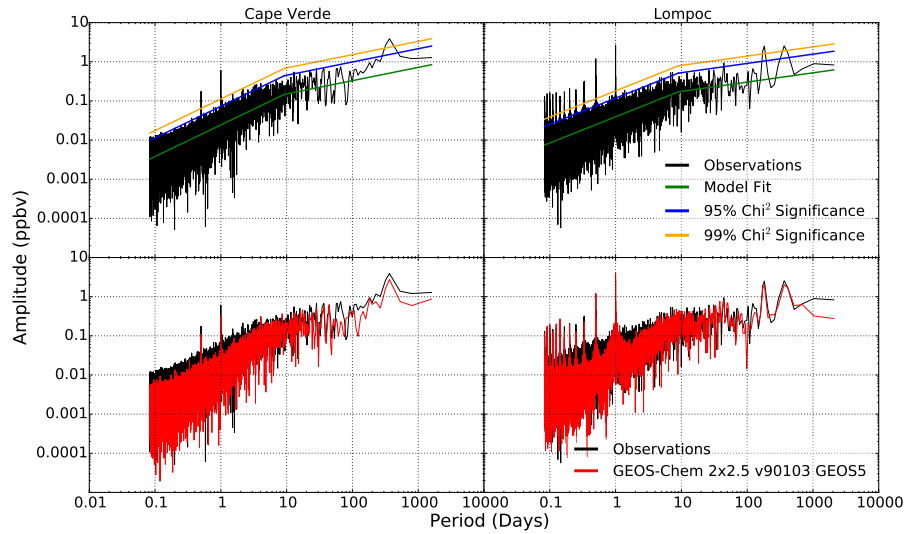
Figure 2. Lomb-Scargle Periodgram spectra for surface O$_3$ at Cape Verde (16.51° N, 24.52° W) and Lompoc (34.73° N, 120.43° W), between 2006-2012. The upper panels shows the observed data spectra together with chi-squared false-alarm levels for significant periodicity based on linear piecewise fits to the spectra. The lower panels compare the spectra of the observations (black) and the GEOS-Chem model (red).
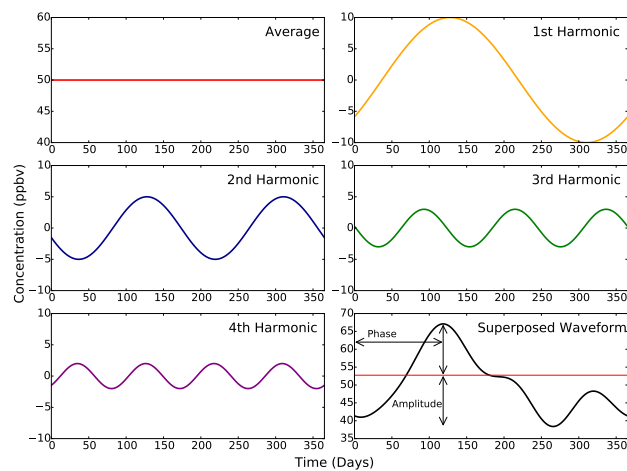
Figure 3. Example of spectral superposition of the average, fundamental frequency and the harmonics for a frequency of interest.
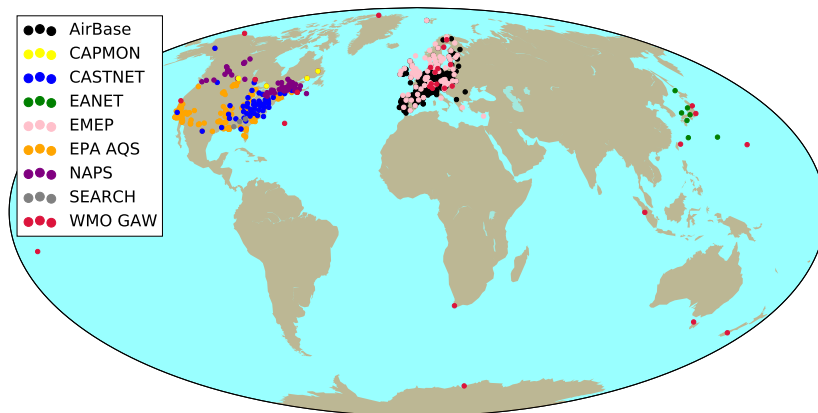
Figure 4. Map of surface sites reporting surface O_3 between 2005-2010 used in this study, coloured by the providing data network.
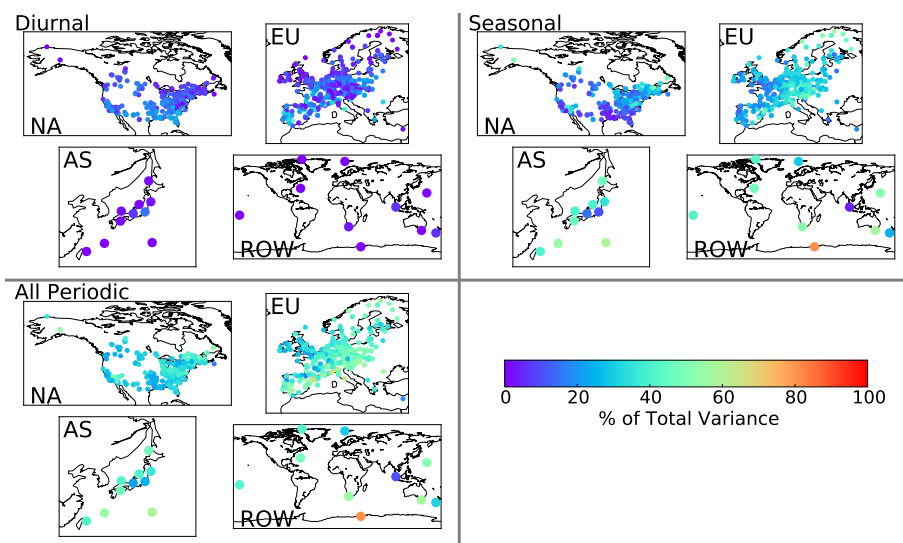
Figure 5. Observational fractional variance of time series by site from diurnal, seasonal and total periodicity.

NA= North America, EU = Europe, AS = Asia, ROW = Rest of World.
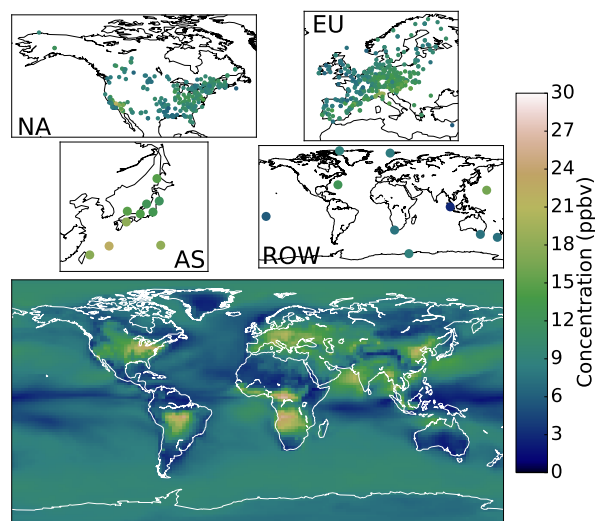
Figure 6. Seasonal amplitudes of observations (upper panels) and model (lower panel).

NA= North America, EU = Europe, AS = Asia, ROW = Rest of World.
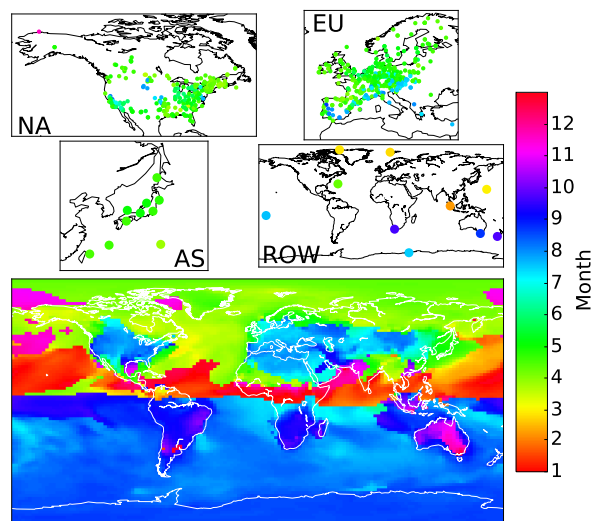
Figure 7. Seasonal phases of observations (upper panels) and model (lower panel).
NA= North America, EU = Europe, AS = Asia, ROW = Rest of World.
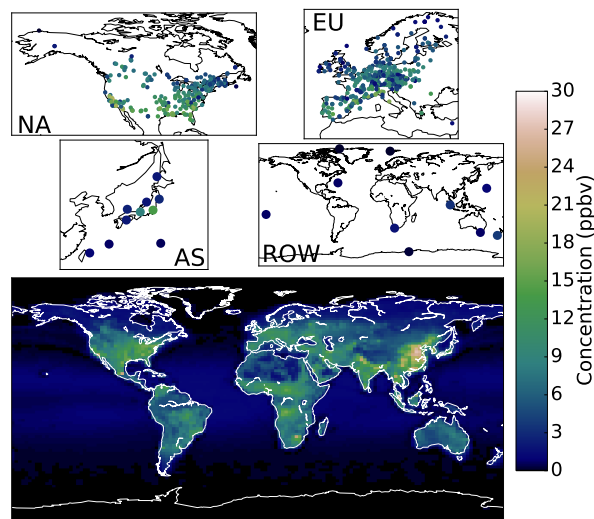
Figure 8. Diurnal amplitudes of observations (upper panels) and model (lower panel).
NA= North America, EU = Europe, AS = Asia, ROW = Rest of World.
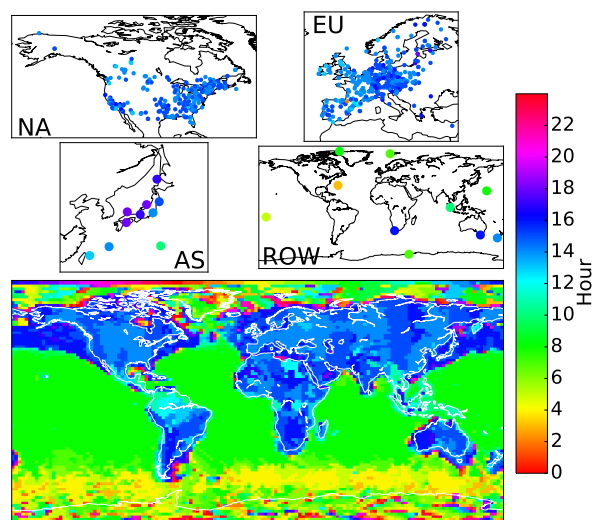
Figure 9. Diurnal phases of observations (upper panels) and model (lower panel).
NA= North America, EU = Europe, AS = Asia, ROW = Rest of World.
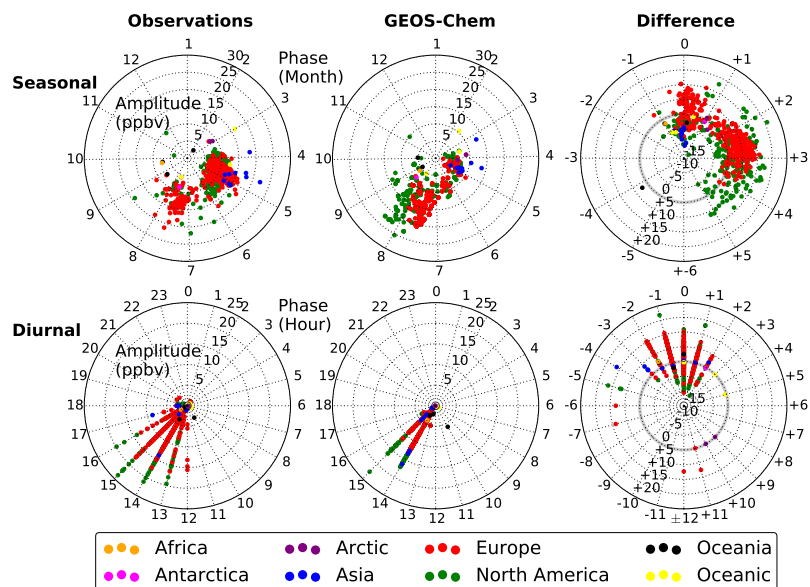
Figure 10. Polar plot of the diurnal and seasonal amplitudes and phases for observations and the GEOS-Chem model, and the differences between them. Circle colour indicates the location of the site.
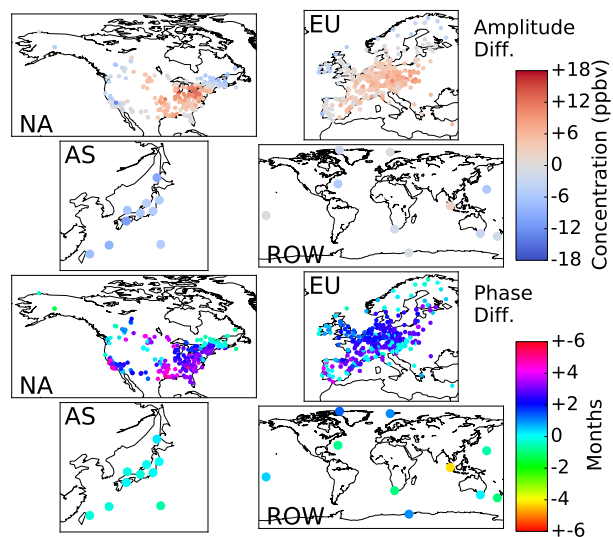
Figure 11. Seasonal amplitude (upper panel) and phase (lower panel) differences between observations and the GEOS-Chem model. NA= North America, EU = Europe, AS = Asia, ROW = Rest of World.
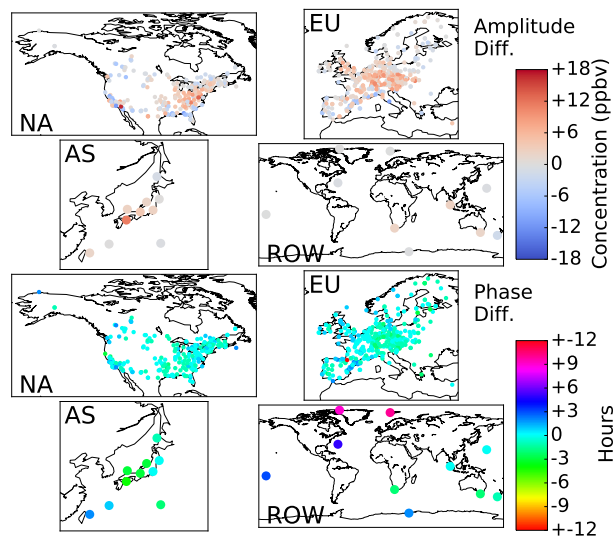
Figure 12. Diurnal amplitude (upper panel) and phase (lower panel) differences between observations and the GEOS-Chem model. NA= North America, EU = Europe, AS = Asia, ROW = Rest of World.
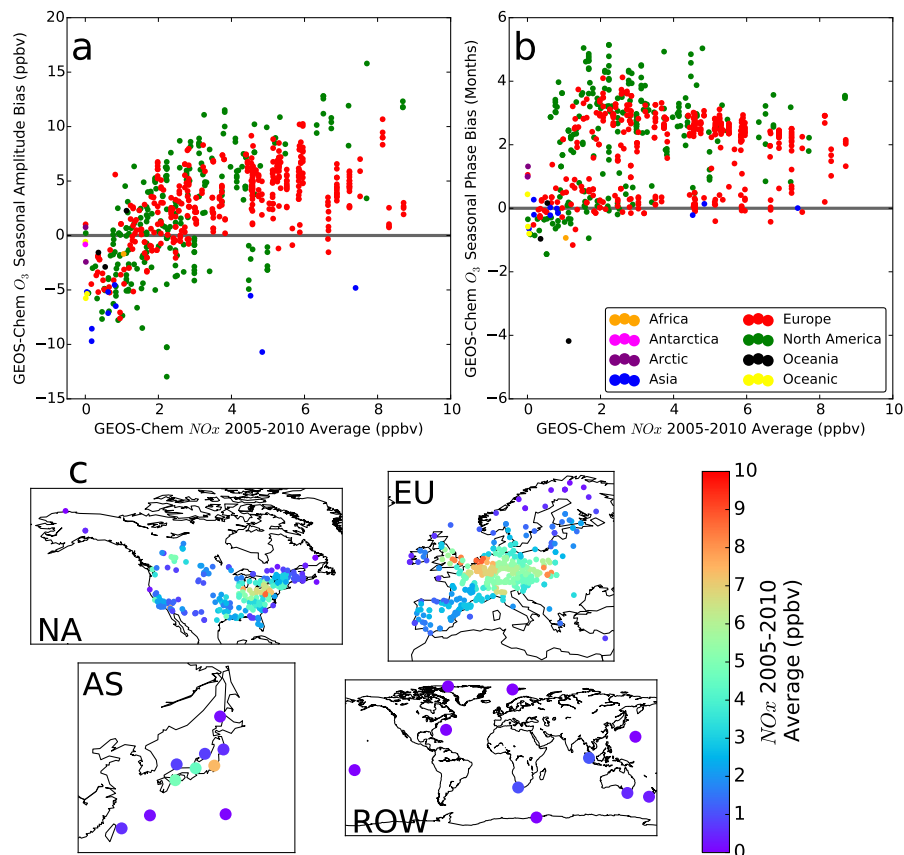
Figure 13. (a) Seasonal amplitude bias vs 2005-2010 Average GEOS-Chem model NO_X, (b) Seasonal phase bias vs 2005-2010 Average GEOS-Chem model NO_X, (c) 2005-2010 Average GEOS-Chem model NO_X by observational site.

NA= North America, EU = Europe, AS = Asia, ROW = Rest of World.